

ARTICLE OPEN

Quantum critical behavior in the asymptotic limit of high disorder in the medium entropy alloy NiCoCr_{0.8}Brian C. Sales¹, Ke Jin¹, Hongbin Bei¹, John Nichols¹, Matthew F. Chisholm¹, Andrew F. May¹, Nicholas P. Butch^{2,3}, Andrew D. Christianson⁴ and Michael A. McGuire¹

The behavior of matter near a quantum critical point is one of the most exciting and challenging areas of physics research. Emergent phenomena such as high-temperature superconductivity are linked to the proximity to a quantum critical point. Although significant progress has been made in understanding quantum critical behavior in some low dimensional magnetic insulators, the situation in metallic systems is much less clear. Here, we demonstrate that NiCoCr_x single crystal alloys are remarkable model systems for investigating quantum critical point physics in a metallic environment. For NiCoCr_x alloys with $x \approx 0.8$, the critical exponents associated with a ferromagnetic quantum critical point are experimentally determined from low temperature magnetization and heat capacity measurements. All of the five exponents ($\gamma_T \approx 1/2$, $\beta_T \approx 1$, $\delta \approx 3/2$, $\nu z_m \approx 2$, $\bar{\alpha}_T \approx 0$) are in remarkable agreement with predictions of Belitz–Kirkpatrick–Vojta theory in the asymptotic limit of high disorder. Using these critical exponents, excellent scaling of the magnetization data is demonstrated with no adjustable parameters. We also find a divergence of the magnetic Gruneisen parameter, consistent with a ferromagnetic quantum critical point. This work therefore demonstrates that entropy stabilized concentrated solid solutions represent a unique platform to study quantum critical behavior in a highly tunable class of materials.

npj Quantum Materials (2017)2:33; doi:10.1038/s41535-017-0042-7

INTRODUCTION

The connection between quantum fluctuations in the vicinity of a quantum critical point (QCP) and emergent ground states, such as high-temperature superconductivity, remains a topic of great interest in the condensed matter physics community.^{1–5} One key to making progress in this area is the identification of model material systems that are complex enough to exhibit the physics of interest but simple enough to be compared to theory. Studies of several low dimensional magnetic materials have greatly improved our understanding of QCP physics in insulating solids,^{6–8} but our understanding of QCP phenomena in metallic systems is much less clear.^{2, 9, 10} One hindrance is that few systems are microscopically homogeneous near the QCP, due to the need for small concentrations of dopants, and this can disrupt the feedback loop between theory and experiment.

The NiCoCr_x alloys (with $x \approx 1$) are related to the recently discovered high-entropy-alloys, such as NiCoCrFeMn,^{11, 12} where configurational entropy stabilizes a random distribution of elements on a simple face-centered cubic lattice (fcc). These alloys have been shown to be chemically homogeneous from the centimeter to the nanometer scale. An example of an atomic resolution scanning transmission electron microscope (STEM) image from a NiCoCr single crystal is shown in Fig. 1. No clustering of any of the three elements is observed. Energy dispersive spectroscopy data for the NiCoCr_{0.8} and NiCoCr crystals presented in Fig. S1 illustrate chemical homogeneity on the micron scale.

The high-entropy-alloys have remarkable mechanical properties,¹³ and enhanced resistance to radiation damage.¹⁴ The alloys are also unusual because all elements have roughly equal concentrations and the dilute impurity approximation is invalid. A recent theoretical model based on enthalpies of formation coupled with entropy stabilization successfully predicts which combination of elements will form a single-phase solid solution.¹⁵ The composition NiCoCr also has remarkable mechanical properties at cryogenic temperatures and has been termed a medium-entropy alloy.¹⁶

Here we report low temperature magnetization and heat capacity for single crystals of the concentrated solid solutions NiCoCr_x with $x \approx 0.8$ as a function of temperature and magnetic field. The extreme chemical disorder in these alloys is an essential component of the physics, suppressing a first order ferromagnetic transition that invariably occurs in many other potential ferromagnetic quantum critical point (FQCP) systems.⁹ In carefully prepared single crystals with electropolished surfaces and minimum mechanical damage, we find that the BKV theory^{17, 18} of metallic ferromagnetic QCPs provides an excellent description of all of our data. The approximate temperature–magnetic field phase diagram that describes the boundary between the quantum critical and the Fermi liquid regions is also determined for the NiCoCr_{0.8} composition from magnetization data. Finally we demonstrate that the magnetic Gruneisen parameter [$\Gamma = (dM/dT)/C_p$] diverges, another indication of a FQCP. These findings open the door to the study of QCP physics in a new and flexible class of model materials.

¹Materials Science and Technology Division, Oak Ridge National Laboratory, Oak Ridge, TN, USA; ²NIST Center for Neutron Research, National Institute of Standards and Technology, Gaithersburg, MD, USA; ³Center for Nanophysics and Advanced Materials, Department of Physics, University of Maryland, College Park, MD, USA and ⁴Quantum Condensed Matter Division, Oak Ridge National Laboratory, Oak Ridge, TN, USA
Correspondence: Brian C. Sales (salesbc@ornl.gov)

Received: 23 March 2017 Revised: 6 June 2017 Accepted: 12 June 2017
Published online: 29 June 2017

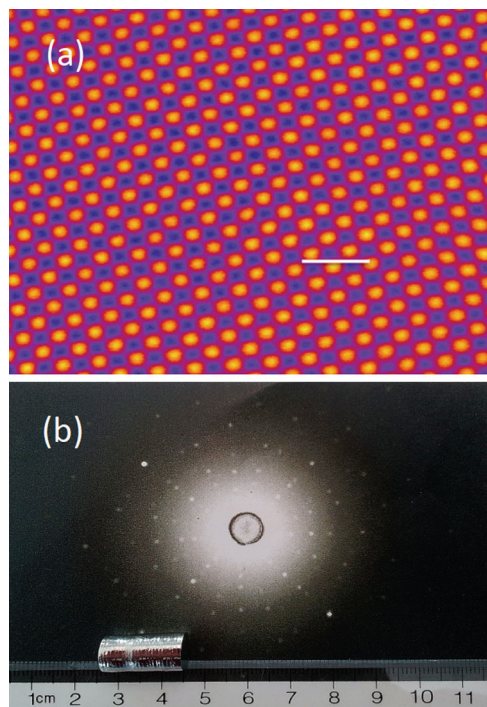


Fig. 1 Homogeneous NiCoCr_x Crystals **a** STEM image of columns of atoms along the [100] direction from a NiCoCr single crystal. These images and associated EELS (electron energy loss spectroscopy) data taken at the same time do not detect any evidence of elemental clustering or ordering. Each “atom” in the figure is actually a column of atoms about 20 nm in length. The white scale bar corresponds to 0.5 nm. Clustering of Cr atoms would, for example, produce regions of lower image intensity. The distance between columns is approximately 0.18 nm, and this would also vary if significant clustering occurred. The images were obtained using a Nion UltraSTEM200 operated at 200 kV with an illumination half-angle of 30 mrad and an inner detector half-angle of 65 mrad. **b** Laue X-ray image from a 10 g NiCoCr_{0.8} crystal shown at the bottom

RESULTS

As is illustrated in Fig. 2, NiCoCr_{0.8} is close to the Cr concentration where the ferromagnetic transition temperature, T_c , goes to zero. The ferromagnetism is highly itinerant for all compositions $x > 0.5$; for values of $x \approx 0.6$ the saturation moment per atom is $0.15 \mu_B$, $T_c = 75 \pm 2$ K, and the Rhodes–Wohlfarth ratio is 8.5.¹⁹ For increasing Cr concentrations, x , there is a rapid nearly exponential decrease in T_c , and in addition to the rapid depression of T_c , increasing the Cr concentration introduces a type of frustration since the spins on the Cr atoms want to be antiparallel to neighboring Ni, Co, and Cr spins, which cannot be satisfied on a fcc lattice. For Cr concentrations greater than $x \approx 0.4$, theory (KKR–CPA)^{14, 19, 20} greatly over-estimates both the spontaneous magnetic moments and T_c (see Fig. 3c. Ref. 19) indicating significant effects that are not captured by density functional theory. This deviation from theory and the observation of $T_c \rightarrow 0$ K motivate a detailed characterization of the critical behavior and exponents for compositions near NiCoCr_{0.8}.

The low field and low temperature magnetization data from a NiCoCr_{0.8} single crystal are shown in Fig 3a. The divergence of the low field susceptibility, $\chi = (M/H)$ as T approaches zero determines the critical exponent γ_T , where $\chi \propto T^{-\gamma_T}$. For low applied magnetic fields from 0.0001 to 0.1 Tesla, the susceptibility of NiCoCr_{0.8} crystals diverge with $\gamma_T \approx 0.5$. It is important to note that to observe this behavior the surface of the crystals had to be electropolished and carefully cleaned before magnetic

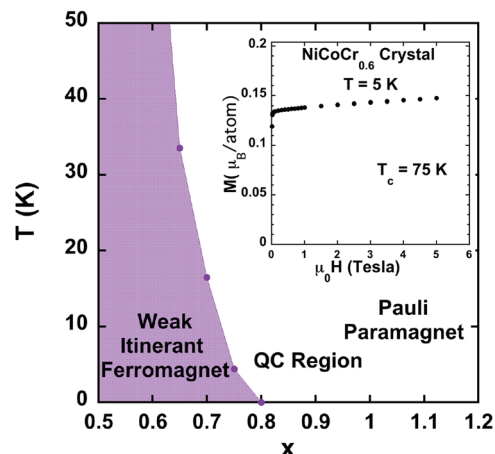


Fig. 2 Phase diagram of NiCoCr_x alloys. Illustration of the rapid non-linear decrease in Curie temperature, T_c , with chromium concentration, x . The Curie temperatures for each composition are estimated from Arrott plots, the maximum in $-dM/dT$ with $H = 100$ Oe, or extrapolation of M^2 vs T with $H = 100$ Oe. The T_c 's determined by each method are self-consistent within an error of about ± 2 K. (see ref 19 for additional details). The inset shows a magnetization curve for a NiCoCr_{0.6} crystal at 5 K. The small value of the spontaneous moment indicates highly itinerant ferromagnetism

measurements (see experimental section), otherwise the magnetic response is dominated by extrinsic defects.

The critical exponent, δ , is determined from the critical isotherm in the limit that $T \rightarrow 0$ K and is defined as $M(T, H) \propto H^{1/\delta}$. Although technically δ is only defined at T_c (which is 0 at the FQCP), the values are expected to saturate at a low enough temperature. Magnetization isotherms at our lowest temperature of 1.8 K are displayed in Fig. 3b for two NiCoCr_{0.8} crystals. Power law fits to these data yield an estimate of $\delta = 1.55 \pm 0.1$.

The critical exponent, β_T , can be formally associated with a FQCP and is defined in terms of the order parameter M in the limit of $H \rightarrow 0$ and $T \rightarrow 0$ as proportional to T^{β_T} . The proportionality constant is of course zero at the FQCP since the spontaneous magnetization is only non-zero in the ordered magnetic phase. In this case the value of β_T can be estimated by tuning the Cr composition slightly away from the critical value of $x \approx 0.8$ and into the ferromagnetic state ($x < 0.8$, see Fig. 2) and then determine the values of β_T as $x = 0.8$ is approached. This was done for 3 polycrystalline NiCoCr_x samples with $x = 0.75, 0.70, 0.65$ and T_c 's of 4.4, 16.5, and 33.5 K. These values for T_c were defined by the maximum in $-dM/dT$ with $H = 100$ Oe. This definition of T_c appeared to be the least subject to assumptions. We note however that changing T_c by a couple of degrees did not significantly effect the results for β_T . The evolution of the magnetization below T_c is evaluated for each of the three alloys with a small applied field of $H = 100$ Oe. For each alloy the magnetization data below T_c was fit to a power law for various values of $T_c - T$, with the assumption that the correct value of β_T is attained as $T_c - T$ approaches zero (Fig. 3c). Using this analysis, we obtain the value of β_T for each alloy. These values are plotted in Fig. 3d and yield an approximate value for β_T ($x \approx 0.8$) of 1.

Taken together, direct analysis of the magnetization data for NiCoCr_{0.8} give the following critical exponents: $\gamma_T \approx 0.5$, $\delta \approx 3/2$, and $\beta_T \approx 1$. The subscript T for γ and β indicate the temperature dependence of the relevant variables when the composition x has been tuned to its critical value ($x_{cr} \approx 0.8$) where the transition temperature is zero. This is also the notation used in the BKV theory^{17, 18}. These experimental values for γ_T , δ , and β_T are also the values predicted from BKV theory in the “dirty” or high-disordered limit. In this limit the Widom relationship $\gamma_T = \beta_T (\delta - 1)$, is expected

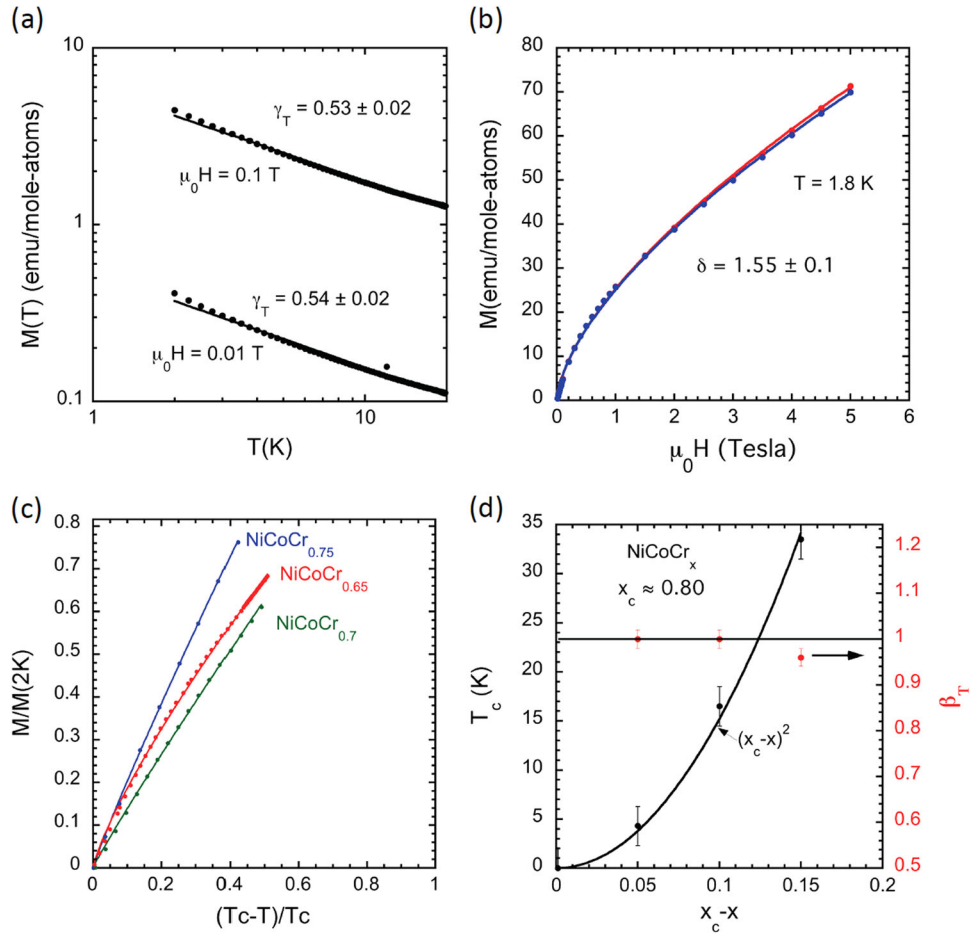


Fig. 3 Critical exponents from magnetization data **a** Magnetization vs temperature for a NiCoCr_{0.8} crystal in applied magnetic fields of $\mu_0 H = 0.01$ and 0.1 Tesla. For these low applied fields the susceptibility, χ , is given by M/H . The *solid lines* are least square fits of the data to a power law $T^{-\gamma_T}$, with the values for γ_T as shown in the figure. The error bars for γ_T correspond to the standard error of the mean (s.e.m.) from multiple samples. **b** magnetization vs applied magnetic field at our lowest temperature for two NiCoCr_{0.8} crystals, and the value of δ determined from these isotherms. The relatively large error bars (s.e.m.) for δ reflect the uncertainty on whether to include the low field magnetization data where domain effects can be important^{22, 24} **c** Increase of the magnetization below T_c with an applied field of 0.01 T for three ferromagnetic polycrystalline samples. The lines are power law fits to all the data shown. Values of β_T are obtained by fits over smaller T_c - T intervals near T_c . The small error bars (s.e.m.) for β_T in panel **d** reflect the insensitivity of the analysis to the exact value chosen for T_c . **d** Curie temperature vs. $(x_c - x)$, where x is the Cr concentration, and x_c is the concentration where $T_c \approx 0$. The error bars (s.e.m.) on T_c reflect the results from different methods used to determine T_c . The solid line is a force fit of the T_c data to $(x_c - x)^2$, the functional dependence expected from BKV theory. The values of the critical exponent β_T as estimated for the same ferromagnetic samples $x = 0.75, 0.7, 0.65$. (1 emu = 1 mA m² in SI units)

to hold¹⁸ and within our experimental error it does. This means that only two of the three exponents are independent. In the “dirty” limit, BKV theory¹⁸ also predicts that the Curie temperature should increase rapidly as the composition is tuned away from the critical composition as $T_c \propto (x_c - x)^{1/z_m} = (x_c - x)^2$, since $z_m = 2$ and $\nu = 1$ (from the theory). Although we do not have enough experimental data to show that $z_m \nu$ is exactly two, a force fit of the T_c data to $(x_c - x)^2$ does provide a good description of our data as shown in Fig. 3d.

One test of quantum critical behavior is the divergence of the magnetic Gruneisen parameter²¹ (also called the magnetocaloric ratio), $\Gamma = (dM/dT)/C_p$, as T approaches 0.^{10, 22, 23} Low temperature heat capacity data from NiCoCr_{0.8} with $H = 0$ are displayed in Fig. 4a. At the lowest temperatures C_p is proportional to T^α with a value of $\alpha = 0.92$, which implies that C_p/T weakly diverges as $T^{-0.08}$. This weak divergence of C_p/T is close to the exponent value of $\bar{\alpha}_T = 0$ expected from BKV theory. As noted above, the low field ($H = 100$ Oe) susceptibility (M/H), diverges as $\approx T^{-0.5}$, which implies that dM/dT diverges as $\approx T^{-3/2}$. Thus Γ diverges as $\approx T^{-2.5}$. This low temperature divergence is demonstrated in Fig. 4b, using either the total measured heat capacity or just the electronic/magnetic

portion. For the three ferromagnetic compositions ($x = 0.75, 0.7, 0.65$), the low temperature magnetic Gruneisen parameter approaches 0 since in low applied magnetic fields $dM/dT \rightarrow 0$.

The scaling of the magnetization data, $M(T, H)$, are determined by the critical exponents.^{22, 24} All of the magnetization data from the NiCoCr_{0.8} single crystals should collapse onto a single curve when M/T^{β_T} is plotted vs. $H/T^{\gamma_T + \beta_T}$. Since γ_T and β_T for NiCoCr_{0.8} are found experimentally to have the values of $\gamma_T \approx 0.5$, and $\beta_T \approx 1$, this implies that if $M(T, H)/T$ is plotted vs. $H/T^{1.5}$, all of the magnetization data should fall on one curve. This is indeed the case as illustrated in Fig. 5. It is important to emphasize that we are not using the scaling plots to extract precise values for γ_T and β_T , but rather we simply illustrate that the values found do result in excellent scaling. It has been demonstrated recently that it is very difficult to extract unique values of critical exponents from scaling plots alone.²²

DISCUSSION

We have provided strong evidence that NiCoCr_{0.8} is close to a FQCP and the experimentally determine critical exponents

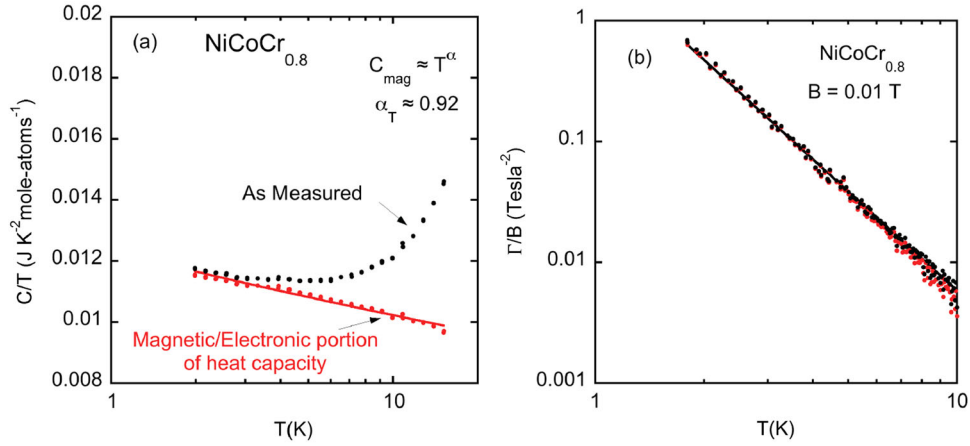


Fig. 4 Heat capacity data and illustration of divergence of magnetic Grüneisen coefficient **a** Heat capacity data divided by temperature vs $\log T$. The lattice contribution is estimated using a NiCoCr_{1.2} alloy and it is subtracted from the total measured heat capacity for NiCoCr_{0.8} resulting in the data shown in *red*. This alloy is a Pauli paramagnet outside of the critical region (see Fig. 2) that should have a very similar phonon contribution to the heat capacity.¹⁹ The low temperature heat capacity of the reference alloy, NiCoCr_{1.2}, is well described by a Debye model with an electronic contribution characterized by $\gamma = 9.2$ mJ/mole-K², and $\Theta_D = 466$ K. **b** $\log(\Gamma)$ vs. $\log(T)$, with a solid line illustrating the divergence of $\Gamma \approx T^{-2.5}$. The standard deviation (s.d.) for these data are approximately the size of each data point

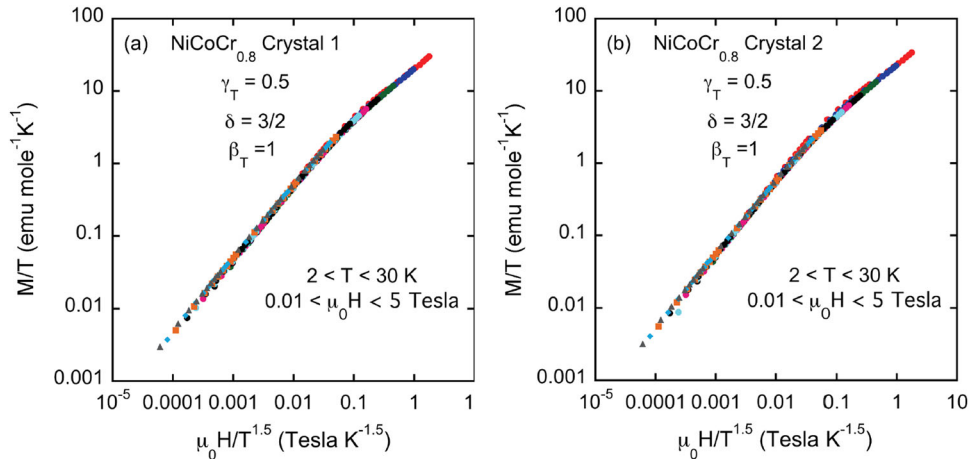


Fig. 5 Demonstration of excellent scaling of magnetization data from two crystals **a**, **b** of NiCoCr_{0.8} using the experimentally determined values of $\gamma_T \approx 0.5$, and $\beta_T \approx 1$. There are no adjustable parameters

($\gamma_T \approx 0.53 \pm 0.02$, $\beta_T \approx 1 \pm 0.02$, $\delta \approx 1.55 \pm 0.1$, $v_{z_m} = 2$, $\bar{\alpha}_T = 0.08$) are close to the values expected from BKV theory in the asymptotic limit of high-disorder ($\gamma_T = 1/2$, $\beta_T = 1$, $\delta = 3/2$, $v_{z_m} = 2$, $\bar{\alpha}_T = 0.0$). In the limit of high disorder, effects due to Griffiths phases are possible particularly in the paramagnetic region. The BKV theory¹⁸ does not consider Griffith phases and the good agreement between our data and the BKV model would suggest that Griffith phase effects are small in the NiCoCr_{0.8} alloys. This is also the conclusion from ac susceptibility measurements shown in Figure S2.

Magnetic field, which can be thought of as another variable perpendicular to the temperature and Cr composition axis (Fig. 2), is used to probe the extent of the quantum critical region away from the FQCP of the NiCoCr_{0.8} alloy. As a magnetic field is applied to NiCoCr_{0.8} the magnetic fluctuations are suppressed and the system is tuned toward a normal Fermi liquid with a Pauli susceptibility. This behavior suggests there is a region where the system's behavior is governed by quantum fluctuations, as opposed to thermally-induced fluctuations, consistent with the existence of quantum critical behavior in NiCoCr_{0.8}. This crossover from the quantum critical regime to the Fermi liquid regime occurs at T^* for a given applied magnetic field B . Experimentally

the crossover temperature T^* is usually estimated as the temperature where a maximum occurs in $\chi(T)$, with $\chi = dM/dH$ extracted from DC magnetization curves at fixed temperatures or from ac susceptibility data^{10, 23} such as shown in Fig. 6a. The dependence of T^* on applied magnetic field B is shown in Fig. 6b. A power law fit to T^* vs B gives $T^* = 5.62 B^{0.67}$ (or $T^* \approx 1.5$ vs B) the same scaling variable used in Fig. 5. This provides another self-consistency check that the analysis of the magnetization data from NiCoCr_{0.8} in terms of a FQCP is reasonable.

As noted previously in reference,¹⁹ the residual resistivity, ρ_0 , of the NiCoCr_x alloys is high, of the order of 80 $\mu\Omega$ cm, and for many of the alloys with $x \approx 0.8$ the resistivity is linear down to at least 1.0 K. A large value of ρ_0 is not considered in the BKV analysis presented in reference,¹⁸ and for that reason resistivity data were not discussed in the main portion of the manuscript. However, the electrical resistivity of a NiCoCr_{0.8} crystal in various magnetic fields is shown in Figure S3, along with the temperature-magnetic field scaling behavior of the data, which is close to that presented in Fig 6.

As briefly discussed in the experimental section, strain can also be used as another tuning variable, though we have not developed a strain-based phase diagram to complement Fig. 6b.

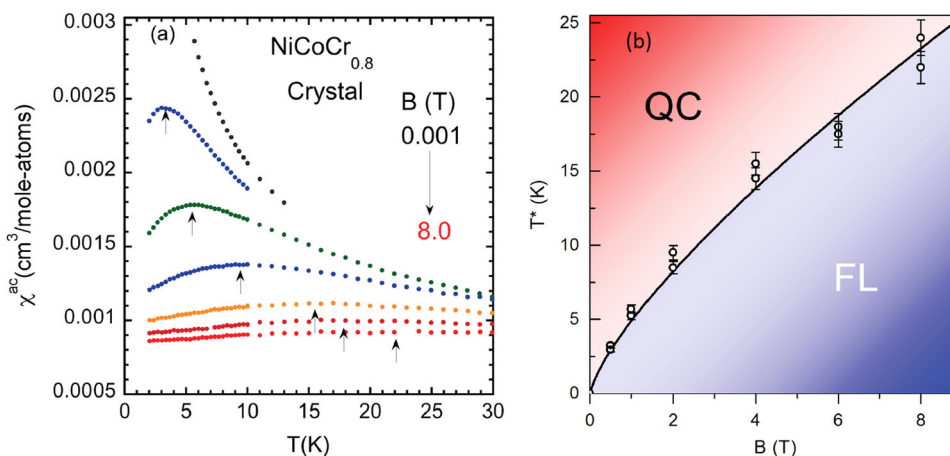


Fig. 6 Field induced crossover from quantum critical to Fermi liquid regimes **a** ac susceptibility vs. temperature with applied dc magnetic fields between 0.001 and 8 Tesla. The *black arrows* denote the approximate values of T^* for a fixed dc magnetic field. **b** The crossover temperature, T^* , as a function of magnetic field for a NiCoCr_{0.8} single crystal as determined from both DC magnetization and ac susceptibility data. The error in T^* reflects the uncertainty in determining the temperature of the maximum using either ac or dc susceptibility data. The regions dominated by quantum critical (QC) and Fermi liquid (FL) behavior are noted in the figure. The *black line* is a power law fit to the data: $T^* = 5.62 B^{0.67 \pm 0.05}$ where the error bars are the standard deviation from least squares fitting

Since there are well over two hundred ternary concentrated solid solutions with compositions ABC predicted to form,¹⁵ this class of entropy stabilized alloys represents an interesting new class of tunable materials for the investigation of quantum critical behavior.

METHODS

Single crystals of NiCoCr_{0.8} are grown in an optical floating zone furnace. Polycrystalline rods for the crystal growth are produced by arc-melting stoichiometric amounts (1:1:0.8) of high purity (>99.9%) Ni, Co, and Cr in an argon atmosphere followed by drop casting into a copper mold.²⁵ Laue back reflection and X-ray diffraction measurements indicated single crystals with a small mosaic spread ($\approx 0.4^\circ$). Crystals suitable in size for magnetization (≈ 200 mg) or heat capacity (≈ 25 mg) are cut from a large single crystal boule using an electro-discharge machine. To eliminate the damage layer created after cutting or sanding, the crystals are electropolished in an 85% H₃PO₄ solution with approximately a 10 V bias. This surface preparation is essential, particularly for the magnetic measurements. If, for example, the samples are cut with a low speed diamond saw and then polished with SiC sandpaper, or just cut with a diamond saw, it is found that the temperature dependence and magnitude of the low field magnetic susceptibility is dramatically altered- by more than a factor of two. We also find that severe coldworking the material increases the low temperature susceptibility by about a factor of ten. These results suggest that strain and pressure may also be a useful QCP tuning parameter for the NiCoCr_{0.8} alloys, although that is beyond the scope of the present work. The chemical homogeneity of crystals grown this way have been checked on the micron scale using energy dispersive spectroscopy measurements and on the nanoscale using atom probe measurements.²⁵ To further examine both the crystalline perfection and the chemical homogeneity we perform atomic resolution STEM measurements and single column electron energy loss spectroscopy (EELS) on a NiCoCr single crystal. The STEM results, shown in Fig. 1, confirm the crystalline perfection and the absence of clustering of any of the elements.

The DC and AC magnetic measurements are made using a commercial SQUID magnetometer (Magnetic Property Measurement System from Quantum design) and the ac susceptibility option of a Physical Property Measurement System (PPMS) (also from Quantum Design), respectively. To check for possible glassy magnetic behavior, both zero-field-cooled and field-cooled measurements are performed. Within experimental error there is no difference in the magnetization data at all fields. As a further check, ac susceptibility measurements are made as a function of frequency, and no glassy behavior could be detected (Figure S2). Heat capacity

measurements are made using the PPMS heat capacity option. Identification of commercial equipment does not imply endorsement by National Institute of Standards and Technology.

Data availability

All relevant data are available from the authors.

ACKNOWLEDGEMENTS

It is a pleasure to acknowledge helpful discussions with Jamie Morris, Lekh Poudel, Malcolm Stocks, German Samolyuk, Claudia Troparevsky and Jiaqiang Yan. I particularly want to thank Claudia Troparevsky for providing an extensive list of predicted ternary solid solution alloys using the methodology developed in reference¹⁵. This research was supported primarily by the Department of Energy, Office of Science, Basic Energy Sciences, Materials Sciences and Engineering Division (B.C.S., J.N., A.F.M., M.F.C., M.A.M.). K.J. and H.B. were supported by the Energy Dissipation to Defect Evolution (EDDE), an Energy Frontier Research Center funded by the U. S. Department of Energy, Office of Science, BES. Research at ORNL's Spallation Neutron Source was supported by the Scientific User Facilities Division, Office of Basic Energy Sciences, U. S. Department of Energy (A.C.).

AUTHOR CONTRIBUTIONS

B.C.S. conceived the experiments, and made most of the transport, magnetic, and heat capacity measurements with help from A.F.M., M.A.M., and J. N. K. J. and H. B. grew, oriented, cut, and electropolished the crystals. M.F.C. took and analyzed atomic resolution STEM and EELS data. A.C. and N.B. made key contributions to the analysis of the data. All authors contributed to the preparation of the manuscript.

ADDITIONAL INFORMATION

Supplementary Information accompanies the paper on the *npj Quantum Materials* website (doi:10.1038/s41535-017-0042-7).

Competing interests: The authors declare that they have no competing financial interests.

Publisher's note: Springer Nature remains neutral with regard to jurisdictional claims in published maps and institutional affiliations.

REFERENCES

1. Sachdev, S. *Quantum Phase Transitions*. (Cambridge University Press: NY, 2011).
2. Sachdev, S. & Keimer, B. Quantum criticality, *Phys. Today* **64**, 29–35 (2011).

3. Analytis, J. G., Kuo, H.-H., McDonald, R. D., Wartenbe, M., Rourke, P. M. C., Hussey, N. E. & Fisher, I. R. Transport near a quantum critical point in BaFe₂(As_{1-x}P_x)₂. *Nat. Phys.* **10**, 194–197 (2014).
4. Moriya, T. & Ueda, K. Spin fluctuations and high temperature superconductivity. *Adv. Phys.* **49**, 555–606 (2000).
5. Marel, Dvd et al. Quantum critical behavior in a high-temperature superconductor. *Nature.* **425**, 271–274 (2003).
6. Coldea, R. et al. Quantum criticality in an ising chain: experimental evidence for emergent E-8 symmetry. *Science* **327**, 177–180 (2010).
7. Kinross, W., Fu, M., Munsie, T. J., Dabkowska, H. A., Luke, G. M., Sachdev, S. & Imai, T. Evolution of quantum fluctuations near the quantum critical point of the transverse field ising chain system Co₂Nb₂O₆. *Phys. Rev. X* **4**, 031008 (2014).
8. Ruegg, C. et al. Quantum magnets under pressure: controlling elementary excitations in TiCuCl₃. *Phys. Rev. Lett.* **100**, 205701 (2008).
9. Brando, M., Belitz, D., Grosche, F. M. & Kirkpatrick, T. R. Metallic quantum ferromagnets. *Rev. Mod. Phys.* **88**, 025006 (2016).
10. Matsumoto, Y. et al. Quantum criticality without tuning in the mixed valence compound β-YbAlB₄. *Science* **331**, 316–319 (2011).
11. Cantor, B., Chang, I. T. H., Knight, P. & Vincent, A. J. B. Microstructural development in equiatomic multicomponent alloys. *Mat. Sci. Eng. A* **375–377**, 213–218 (2004).
12. Wu, Z., Bei, H., Otto, F., Pharr, G. M. & George, E. P. Recovery, recrystallization, grain growth and phase stability of a family of FCC-structured multicomponent equiatomic solid solution alloys. *Intermetallics* **46**, 131–140 (2014).
13. Gludovatz, B., Hohenwarter, A., Catoor, D., Chang, E. H., George, E. P. & Ritchie, R. O. A fracture-resistant high-entropy alloy for cryogenic applications. *Science* **345**, 1153–1158 (2014).
14. Zhang, Y. et al. Influence of chemical disorder on energy dissipation and defect evolution in nickel and nickel-based concentrated solid solution alloys. *Nat. Comm* **6**, 8736–8744 (2015).
15. Troparevsky, C. M., Morris, J. R., Kent, P. R. C., Lupini, A. R. & Stocks, G. M. Criteria for predicting the formation of single-phase high-entropy alloys. *Phys. Rev. X* **5**, 011041 (2015).
16. Gludovatz, B. et al. Exceptional damage-tolerance of a medium-entropy alloy CrCoNi at cryogenic temperatures. *Nat. Comm.* **7**, 10602 (2016).
17. Belitz, D., Kirkpatrick, T. R. & Vojta, T. First order transitions and multicritical points in weak itinerant ferromagnets. *Phys. Rev. Lett.* **82**, 4707–4710 (1999).
18. Kirkpatrick, T. R. & Belitz, D. Exponent relations at quantum phase transitions with applications to metallic quantum ferromagnets. *Phys. Rev. B* **91**, 214407 (2015).
19. Sales, B. C., Jin, K., Bei, H. B., Stocks, G. M., Samolyuk, G. D., May, A. F. & McGuire, M. A. Quantum critical behavior in a concentrated ternary solid solution. *Sci. Rep.* **6**, 26179 (2016).
20. Stocks, G. M., Temmerman, W. N. & Gyorffy, B. L. Complete solution of the korringa-kohn-rostoker coherent-potential-approximation equations: cu-ni alloys. *Phys. Rev. Lett.* **41**, 339–343 (1978).
21. Zhu, L., Garst, M. & Rosch, A. Q. Si Universally diverging gröneisen parameter and the magnetocaloric effect close to quantum critical points. *Phys. Rev. Lett.* **91**, 066404 (2003).
22. Huang, K. et al. Quantum critical scaling in the disordered itinerant ferromagnet UCo_{1-x}Fe_xGe. *Phys. Rev. Lett.* **117**, 237202 (2016).
23. Wu, L. S., Kim, M. S., Park, K., Tsvelik, A. M. & Aronson, M. C. Quantum critical fluctuations in layered YFe₂Al₁₀. *Proc. Natl Acad. Sci.* **111**, 14088 (2014).
24. Huang, C. L. et al. Anomalous quantum criticality in an itinerant ferromagnet. *Nat. Commun.* **6**, 8188 (2015).
25. Wu, Z., Gao, Z., Bei, Y. F. & Single-crystal, H. Plastic behavior of a single-phase, face-centered-cubic structured, equiatomic FeNiCrCo. *Scr. Mater.* **109**, 108–112 (2015).



Open Access This article is licensed under a Creative Commons Attribution 4.0 International License, which permits use, sharing, adaptation, distribution and reproduction in any medium or format, as long as you give appropriate credit to the original author(s) and the source, provide a link to the Creative Commons license, and indicate if changes were made. The images or other third party material in this article are included in the article's Creative Commons license, unless indicated otherwise in a credit line to the material. If material is not included in the article's Creative Commons license and your intended use is not permitted by statutory regulation or exceeds the permitted use, you will need to obtain permission directly from the copyright holder. To view a copy of this license, visit <http://creativecommons.org/licenses/by/4.0/>.

© The Author(s) 2017